Influence of buoyancy on thermocapillary oscillations in a two-layer system

A. A. Nepomnyashchy and I. B. Simanovskii
Department of Mathematics, Technion–Israel Institute of Technology, 32000 Haifa, Israel
and Minerva Center for Nonlinear Physics of Complex Systems, Haifa, Israel
(Received 29 July 2002; revised manuscript received 11 February 2003; published 1 August 2003)

The influence of buoyancy on thermocapillary oscillations was investigated. Nonlinear simulations of standing Marangoni waves in a real two-layer system of fluids were performed. Both the subcritical and supercritical oscillatory regimes were studied. It was found that buoyancy leads to the regularization and suppression of oscillations. The conditions for observation of different types of instability are discussed.

DOI: 10.1103/PhysRevE.68.026301 PACS number(s): 44.27.+g, 68.03.Cd

I. INTRODUCTION

The thermocapillary effect often plays the dominant role in the dynamics and heat and mass transfer in systems with an interface, especially in the case of thin layers and under microgravity conditions. It is the origin of specific surface-tension-driven (Marangoni) instabilities [1].

It is known that the stability problem for the mechanical equilibrium state in a system with an interface is not self-adjoint (see, e.g., [2]); thus an oscillatory instability is possible. The Marangoni oscillatory instability in a two-layer system was first discovered by Sternling and Scriven [3] in the case of two semi-infinite layers. This case actually corresponds to the limit of high wave numbers k. A detailed analysis of the appearance of oscillatory Marangoni instabilities in the limit $Mk^2 \gg 1$, where M is the Marangoni number, was carried out in [4].

In reality, the critical wave number of the instability is usually of the order of unity. In that case, the criteria for the appearance of the oscillatory instability can be essentially changed in comparison with the limit of high wave numbers [5–7].

An example of a physical system where two-layer oscillations have been predicted is the system *n*-octane–methanol (see [8]). A weakly nonlinear bifurcation analysis [8] reveals a subcritical instability of the mechanical equilibrium state with respect to standing waves. In the case of a subcritical instability, a weakly nonlinear analysis cannot give any prediction concerning finite-amplitude motion.

In the present paper the influence of buoyancy on thermocapillary oscillations is considered. It is shown that the oscillations can be observed only under microgravity conditions. Nonlinear simulations of spatially periodic standing waves in the *n*-octane–methanol system are performed. Both the subcritical and supercritical oscillatory regimes are investigated.

The paper is organized as follows. In Sec. II, the mathematical formulation of the problem is presented. The linear stability of the system is analyzed in Sec. III. Nonlinear simulations of the finite-amplitude convective regimes are given in Sec. IV. Section V contains some concluding remarks.

II. FORMULATION OF THE PROBLEM

We consider a system of two horizontal layers of immiscible viscous fluids with different physical properties (see Fig. 1). The system is bounded from above and from below by two isothermic rigid plates kept at different constant temperatures (the total temperature drop is θ). It is assumed that the interfacial tension σ decreases linearly with increasing temperature: $\sigma = \sigma_0 - \alpha T$, where $\alpha > 0$. The dependence of the interfacial tension on the temperature can lead to the onset of the Marangoni instability.

It is known that there are two kinds of Marangoni instability [1,2]. The first type of instability, which occurs in relatively thick layers, develops without a significant deformation of the interface. Another type of instability, which is observed in very thin layers, is caused by the interfacial deformation.

The Sternling-Scriven oscillatory instability studied in the present paper belongs to the first type of instability. We will disregard the deformation of the interface in our analysis. The conditions when the deformational instability can be ignored are considered in Sec. III.

All variables referring to the top layer are marked by the index 1, and the variables referring to the bottom layer are marked by the index 2. Let us use the following notation:

$$\rho = \rho_1/\rho_2, \quad \nu = \nu_1/\nu_2, \quad \eta = \eta_1/\eta_2, \quad \kappa = \kappa_1/\kappa_2,$$

$$\chi = \chi_1/\chi_2, \quad \beta = \beta_1/\beta_2, \quad a = a_2/a_1.$$

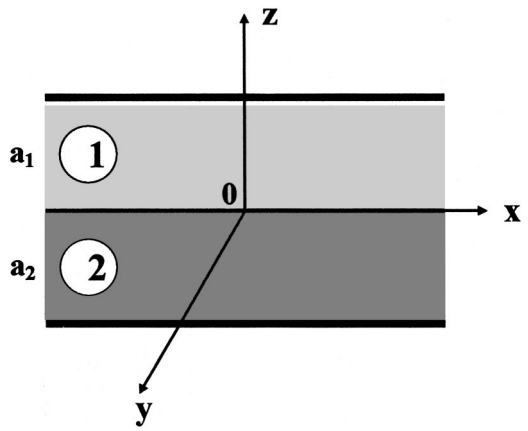

FIG. 1. Geometrical configuration of the two-layer system and coordinate axes.

Here ρ_m, ν_m, η_m, κ_m, χ_m, β_m, and a_m are, respectively, the density, kinematic and dynamic viscosities, heat conductivity, thermal diffusivity, thermal expansion coefficient, and thickness of the mth layer ($m=1,2$). As the units of length, time, velocity, pressure, and temperature we choose a_1, a_1^2/ν_1, ν_1/a_1, $\rho_1\nu_1^2/a_1^2$, and θ, respectively.

The complete nonlinear equations of convection for both fluids have the following form [2]:

$$\frac{\partial \vec{v}_m}{\partial t}+(\vec{v}_m\cdot\vec{\nabla})\vec{v}_m=-e_m\vec{\nabla}p_m+c_m\nabla^2\vec{v}_m+b_m\,\mathrm{Gr}\,T_m\vec{\gamma},$$

$$\frac{\partial T_m}{\partial t}+\vec{v}_m\cdot\vec{\nabla}T_m=\frac{d_m}{\mathrm{Pr}}\nabla^2T_m, \tag{1}$$

$$\vec{\nabla}\cdot\vec{v}_m=0.$$

Here, $\vec{v}_m=(v_{mx},v_{my},v_{mz})$ is the velocity vector, T_m is the temperature, and p_m is the pressure in the mth fluid; $b_1=c_1=d_1=e_1=1$; $c_2=1/\nu$, $d_2=1/\chi$, $e_2=1/\rho$; $\mathrm{Gr}=g\beta_1\theta a_1^3/\nu_1^2$ is the Grashof number and $\mathrm{Pr}=\nu_1/\chi_1$ is the Prandtl number for the liquid in layer 1. The conditions on the isothermic rigid horizontal boundaries are

$$v_1=0,\quad T_1=0,\quad \text{for } z=1, \tag{2}$$

$$v_2=0,\quad T_2=s\quad \text{for } z=-a, \tag{3}$$

where $s=1$ corresponds to the case of heating from below and $s=-1$ corresponds to the case of heating from above.

The boundary conditions on the interface $z=0$ include the relations for the tangential stresses

$$\eta\frac{\partial v_{1x}}{\partial z}-\frac{\partial v_{2x}}{\partial z}-\frac{\eta M}{\mathrm{Pr}}\frac{\partial T_1}{\partial x}=0,$$

$$\eta\frac{\partial v_{1y}}{\partial z}-\frac{\partial v_{2y}}{\partial z}-\frac{\eta M}{\mathrm{Pr}}\frac{\partial T_1}{\partial y}=0; \tag{4}$$

the continuity of the velocity field

$$v_1=v_2; \tag{5}$$

the continuity of the temperature field

$$T_1=T_2; \tag{6}$$

and the continuity of the heat flux normal components

$$\kappa\frac{\partial T_1}{\partial z}=\frac{\partial T_2}{\partial z}. \tag{7}$$

Here $M=\alpha\theta a_1/\eta_1\chi_1$ is the Marangoni number.

The problem (1)–(7) for any choice of parameters has the solution

$$\vec{v}_1^{\,0}=\vec{v}_2^{\,0}=\vec{0},\quad p_1^0=p_2^0=0,\quad T_1^0=-s\frac{z-1}{1+\kappa a},$$

$$T_2^0=-s\frac{\kappa z-1}{1+\kappa a} \tag{8}$$

corresponding to mechanical equilibrium.

III. LINEAR STABILITY THEORY

The stability of the mechanical equilibrium can be investigated in the framework of linear stability theory. The boundary value problem (1)–(7) is linearized around the solution (8). The solutions of the linearized problem are presented as a superposition of normal modes characterized by a wave vector $\vec{k}=(k_x,k_y)$ and a complex growth rate $\lambda=\lambda_r+i\lambda_i$:

$$[\tilde{v}_1(z),\tilde{p}_1(z),\tilde{T}_1(z),\tilde{v}_2(z),\tilde{p}_2(z),\tilde{T}_2(z)]\times\exp(ik_xx+ik_yy+\lambda t), \tag{9}$$

where subsequently the tilde will be omitted.

Since the problem is isotropic, the growth rate λ depends only on the wave vector modulus $k=|\vec{k}|$ but not on its direction. That is why it is sufficient to consider only two-dimensional disturbances with $\vec{k}=(k,0)$ which do not depend on the coordinate y. Introducing the stream function disturbances

$$v_{mx}=\psi_m',\quad v_{mz}=-ik\psi_m\quad (m=1,2),$$

where the prime stands for d/dz, and eliminating pressure disturbances in the usual way, we obtain the following boundary value problem:

$$-\lambda D\psi_m=-c_md^2\psi_m+ik\,\mathrm{Gr}\,b_mT_m, \tag{10}$$

$$\lambda T_m-ikA_m\psi_m=\frac{d_m}{\mathrm{Pr}}DT_m\quad (m=1,2), \tag{11}$$

$$\psi_1=\psi_1'=T_1=0\quad \text{for } z=1, \tag{12}$$

$$\psi_2=\psi_2'=T_2=0\quad \text{for } z=-a, \tag{13}$$

$$\eta\psi_1''-\psi_2''-\frac{ik\eta M}{\mathrm{Pr}}T_1=0\quad \text{for } z=0, \tag{14}$$

$$\psi_1'=\psi_2', \tag{15}$$

$$\psi_1=\psi_2=0, \tag{16}$$

$$T_1=T_2, \tag{17}$$

$$\kappa T_1'=T_2', \tag{18}$$

where $D=d^2/dz^2-k^2$, $A_1=dT_1^0/dz=-s/(1+\kappa a)$, and $A_2=dT_2^0/dz=-s\kappa/(1+\kappa a)$ are the dimensionless temperature gradients.

TABLE I. Parameters of *n*-octane ($m=1$) and methanol ($m=2$).

m	ν_m (m^2/s)	η_m (kg/m s)	κ_m (W/m K)	χ_m (m^2/s)	β_m (l/K)
1	8.0×10^{-7}	5.62×10^{-4}	1.50×10^{-1}	1.02×10^{-7}	1.05×10^{-3}
2	7.0×10^{-7}	5.51×10^{-4}	2.15×10^{-1}	1.09×10^{-7}	1.09×10^{-3}

The mechanical equilibrium state (8) is unstable if $\mathrm{Re}\,\lambda(k)>0$ for a certain value of k.

Both monotonic and oscillatory instabilities may occur in a two-layer system. The stability boundary with respect to monotonic disturbances can be found analytically [2].

Later on, we deal with the system *n*-octane–methanol, which is an example of a physical system where the two-layer longitudinal oscillations have been predicted by heating from above ($s=-1$) (see [8]). The physical parameters of the system are given in Table I [9]; the ratios of the parameters are as follows: $\nu=1.14$, $\eta=1.02$, $\kappa=0.698$, $\chi=0.934$, $\beta=0.963$, and $\mathrm{Pr}=7.84$.

A. Pure thermocapillary convection

First, let us discuss the case of pure thermocapillary convection ($\mathrm{Gr}=0$) formerly studied in [8]. For the ratio of layer thicknesses $a=a_0=1.38$, the monotonic instability threshold (at $k=k_m=5.10$) and the oscillatory instability (at $k=k_o=1.94$) coincide.

In the case $a>a_0$, the oscillatory instability is the most ''dangerous'' one. A typical neutral curve is shown in Fig. 2. One can see that a monotonic instability (solid line) occurs for $s>0$ (by heating from below), as $k<k_d$, and for $s<0$ (by heating from above), as $k>k_d$; $k_d\approx3.95$. The absence of the monotonic instability in the long-wave region $k<k_d$ by heating from above is a condition favorable for the appearance of the oscillatory instability. For $a=1.6$, the critical Marangoni number $M_c=2.715\times10^4$ for the oscillatory instability corresponds to $k_c=1.75$. There exists a codimension-2 point (k_*, sM_*) where the frequency of the oscillations tends to zero, and the oscillatory neutral curve (dashed line) terminates in the monotonic one.

In Fig. 3, the dependences of the critical parameters (M_c, k_c) on the ratio of thicknesses a are shown for both oscillatory and monotonic instabilities. Note that the critical Marangoni number for the oscillatory instability has a minimum $M_c=1.76\times10^4$ at $a\approx2.75$.

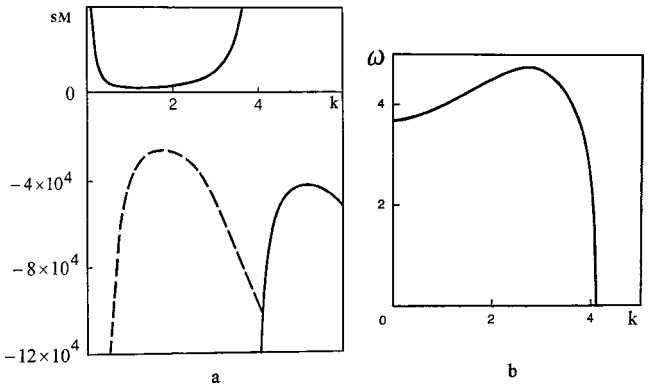

FIG. 2. (a) Neutral stability curves and (b) dependence of the oscillations frequency on the wave number; $a=1.6$.

B. Onset of combined thermocapillary-buoyancy convection (Gr>0)

In the case of heating from below ($s>0$), the combined action of the thermocapillary and buoyancy instability mechanisms leads to a decrease of the critical Marangoni number with the growth of Gr [see Fig. 4(a)]. The point $\mathrm{Gr}=62.6$, $M=0$ corresponds to the excitation of pure buoyancy convection by heating from below. Note that the transition for the pure thermocapillary mechanism of instability to the pure buoyancy one is accompanied by a significant growth of the wave number [see Fig. 4(b)].

In the case of heating from above ($s<0$), the buoyancy effect prevents the onset of thermocapillary convection. Therefore, both monotonic M_m and oscillatory M_o instability thresholds increase with Gr. It is remarkable that the growth of the oscillatory instability threshold is faster than that of the monotonic instability threshold [see Fig. 5(a)]. For $a=1.6$, $M_o=M_m\approx54\,800$ when $\mathrm{Gr}\approx150$. The dependences of the corresponding critical value numbers k_m and k_o are shown in Fig. 5(b).

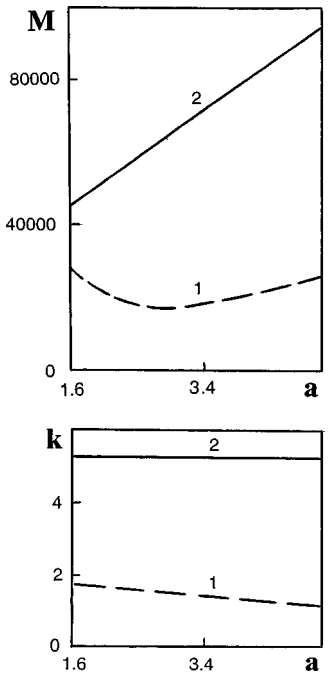

FIG. 3. The dependences of the critical parameter (M_c, k_c) on the ratio of thicknesses a for oscillatory (lines 1) and monotonic (lines 2) instabilities.

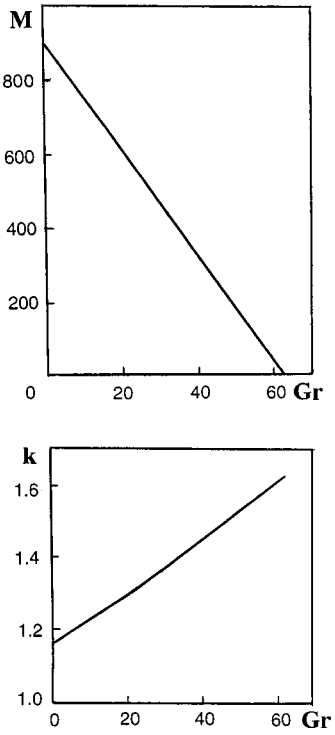

FIG. 4. The dependences of the critical parameter (M_c, k_c) on the Grashof number Gr (heating from below).

C. Deformational instability mode

The results given above were obtained under the assumption that the interface separating the fluids is flàt. Here we discuss the conditions when that assumption is valid.

It is known that the interfacial deformation can lead to the appearance of an additional long-wave stationary instability mode. The threshold of the deformational instability is determined by the formula [see [2], (2.75)]

$$M = s\,\mathrm{Gr}_a \delta \frac{2\,\mathrm{Pr}(1+\eta a)(1+\kappa a)^2 a}{3\kappa(1+a)(1-\eta a^2)}, \tag{19}$$

where

$$\mathrm{Gr}_a = \frac{g a_1^3}{\nu_1^2}, \quad \delta = \frac{\rho_2}{\rho_1} - 1. \tag{20}$$

The influence of buoyancy on the deformational mode is a non-Boussinesq effect, because $\epsilon = \beta\theta = \mathrm{Gr}/\mathrm{Gr}_a$ is the small parameter used in the derivation of the Boussinesq approximation. Thus, it has to be considered only together with other non-Boussinesq corrections, otherwise one can get artifacts (see [10]). Here we shall not consider the problem beyond the Boussinesq approximation.

D. Conditions for observation of the oscillatory instability

As was shown above, there are three competing instability modes: the nondeformational oscillatory instability, the nondeformational stationary instability, and the deformational instability. Let us discuss now the physical conditions for the observation of each type of instability.

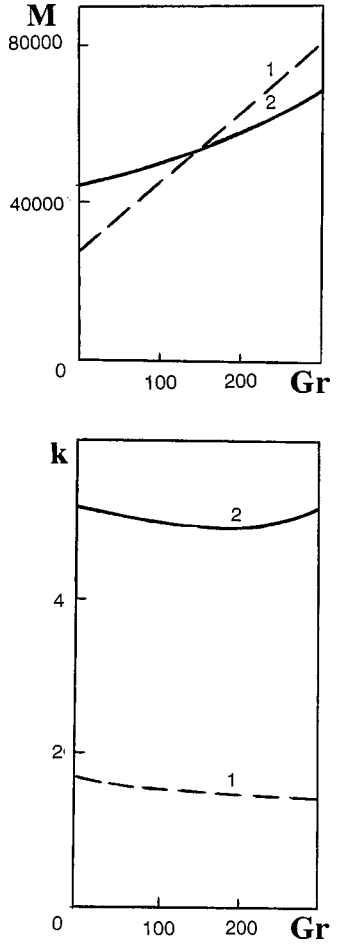

FIG. 5. The dependences of the critical parameter (M_c, k_c) on the Grashof number Gr for oscillatory (lines 1) and monotonic (lines 2) instabilities (heating from above).

First, let us consider the appearance of nondeformational modes. As shown in Sec. III B, the critical parameter is the ratio

$$K = \frac{\mathrm{Gr}}{M} = \frac{\beta_1 \rho_1 \chi_1}{\nu_1 \alpha} g a_1^2.$$

If K is less than K_*, which corresponds to the point $M_o = M_m$, the oscillatory instability is predicted, while in the case $K > K_*$ one expects the appearance of the monotonic instability. For $a = 1.6$, we obtain $K_* = 0.0027$. Substituting the parameters of the *n*-octane–methanol system (see Table I), we find that the oscillatory instability is predicted when $g a_1^2 < 0.115\ \mathrm{cm}^4/\mathrm{s}$. In the case of normal gravity $g = g_0 = 980\ \mathrm{cm/s}^2$ we obtain the condition $a_1 < 0.024$ cm, while in the case $g = g_0 \times 10^{-4}$, $a_1 < 2.4$ cm.

Also, it is necessary to take into account the deformational mode. Substituting the parameters of the *n*-octane–methanol system (see Table I) into Eq. (19) and taking $a = 1.6$, we find that the long-wave deformational instability is developed by heating from above when

$$M \geqslant 4.0 \quad \mathrm{Gr}_a = 6.0 \times 10^7 a_1^3, \tag{21}$$

where a_1 is measured in centimeters. Comparing Eq. (21) with the linear stability threshold of the nondeformational Sternling-Scriven instability, $M=2.715\times10^4$, we find that the deformational instability will appear earlier than the nondeformational one, if $\mathrm{Gr}_a<6800$.

In the case $g=g_0$ that corresponds to $a_1<0.076$ cm, while in the case $g=g_0\times10^{-4}$ we get $a_1<1.6$ cm.

Comparing the results obtained above, we find that in the case $g=g_0$ the oscillatory instability cannot be observed. In the microgravity conditions $g=g_0\times10^{-4}$, the oscillatory instability is predicted in the "window" $1.6<a_1<2.4$ cm. For smaller thicknesses of the top layer, the deformational instability will appear, while for larger thicknesses of the top layer one gets a monotonic nondeformational instability.

IV. TWO-DIMENSIONAL SIMULATIONS OF NONLINEAR CONVECTIVE REGIMES

A weakly nonlinear bifurcation analysis [8] reveals a subcritical instability of the equilibrium state with respect to standing waves, i.e., the instability is not saturated on the level of small-amplitude waves. We have performed nonlinear simulations of nonstationary two-dimensional flows [$v_{my}=0$ $(m=1,2)$; the fields of physical variables do not depend on y]. In this case, we can introduce the stream function ψ,

$$v_{mx}=\frac{\partial\psi_m}{\partial z},\quad v_{mz}=-\frac{\partial\psi_m}{\partial x}\quad (m=1,2).$$

Eliminating the pressure and defining the vorticity as

$$\phi_m=\frac{\partial v_{mz}}{\partial x}-\frac{\partial v_{mx}}{\partial z},$$

we can rewrite the boundary value problem (1)–(7) in the following form:

$$\frac{\partial\phi_m}{\partial t}+\frac{\partial\psi_m}{\partial z}\frac{\partial\phi_m}{\partial x}-\frac{\partial\psi_m}{\partial x}\frac{\partial\phi_m}{\partial z}=c_m\nabla^2\phi_m, \tag{22}$$

$$\nabla^2\psi_m=-\phi_m, \tag{23}$$

$$\frac{\partial T_m}{\partial t}+\frac{\partial\psi_m}{\partial z}\frac{\partial T_m}{\partial x}-\frac{\partial\psi_m}{\partial x}\frac{\partial T_m}{\partial z}=\frac{d_m}{\mathrm{Pr}}\nabla^2T_m\quad (m=1,2), \tag{24}$$

$$\psi_1=\frac{\partial\psi_1}{\partial z}=0,\quad T_1=0\quad \text{for } z=1, \tag{25}$$

$$\psi_2=\frac{\partial\psi_2}{\partial z}=0,\quad T_2=s\quad \text{for } z=-a, \tag{26}$$

$$\psi_1=\psi_2=0,\quad \frac{\partial\psi_1}{\partial z}=\frac{\partial\psi_2}{\partial z},$$

$$\phi_2=\eta\phi_1+\frac{M\eta}{\mathrm{Pr}}\frac{\partial T_1}{\partial x}\quad \text{for } z=0, \tag{27}$$

$$T_1=T_2,\quad \kappa\frac{\partial T_1}{\partial z}=\frac{\partial T_2}{\partial z}. \tag{28}$$

The calculations were performed in a finite region $0<x<L$ with the following types of boundary conditions on the lateral boundaries: (a) periodic boundary conditions

$$\psi_m(x+L,z)=\psi_m(x,z),\quad \phi_m(x+L,z)=\phi_m(x,z),$$

$$\theta_m(x+L,z)=\theta_m(x,z), \tag{29}$$

and (b) rigid heat-insulated boundaries

$$\psi_m=\frac{\partial\psi_m}{\partial x}=\frac{\partial T_m}{\partial x}=0\quad \text{for } x=0,L,\quad m=1,2. \tag{30}$$

The boundary conditions (a) correspond to spatially periodic waves in a laterally infinite two-layer system, and are used for comparison of the numerical results with those of the linear theory developed for the infinite system. The boundary conditions (b) correspond to a closed cavity.

The boundary value problem (22)–(30) was solved by the finite-difference method. The equations and boundary conditions were approximated on a uniform mesh using a second-order approximation for the spatial coordinates. The nonlinear equations were solved using an explicit scheme on a rectangular uniform mesh 56×56. The Poisson equation was solved by the iterative Liebman successive over-relaxation method at each time step; the accuracy of the solution was 10^{-5}. The Kuskova-Chudov formulas [11] providing second-order accuracy were used for approximation of the vorticity on the solid boundaries.

The details of the numerical method can be found in the book by Simanovskii and Nepomnyashchy [2].

A. Pure thermocapillary convection

Periodic boundary conditions

Let us fix the ratio of layer thicknesses $a=1.6$. According to the results of the linear stability theory, $k_c=1.75$, we performed the nonlinear simulations of finite-amplitude oscillatory flow regimes in a cell with the aspect ratio $L=3.6$, which contains exactly one period of the wave.

The prediction of the weakly nonlinear theory is justified. We observed time-periodic standing waves. The characteristic patterns of the stream function isolines and isotherms during one-half of the period are shown in Fig. 6. The flow is symmetric with respect to the vertical lines $x=x_\pm$, $x_+-x_-=L/2$:

$$\psi(x-x_\pm,z,t)=-\psi(x_\pm-x,z,t),$$

$$T(x-x_\pm,z,t)=T(x_\pm-x,z,t). \tag{31}$$

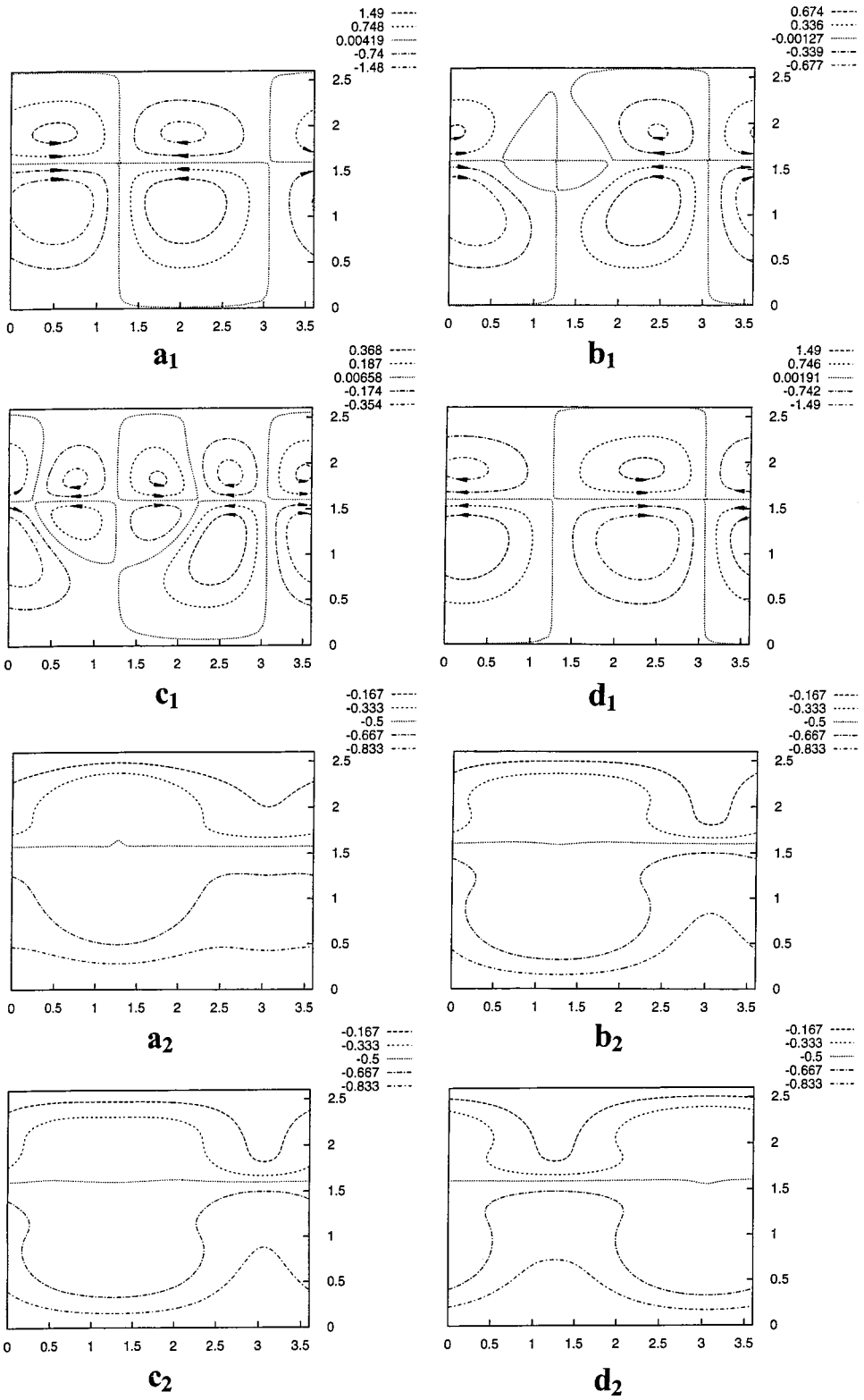

FIG. 6. Streamlines (a1)–(d1) and isotherms (a2)–(d2) for the symmetric time-periodic motion in the region with $L=3.6$; $M=3.07\times10^4$.

The position of the vertical symmetry lines is determined by the initial conditions. The typical structure contains two vortices of different signs per spatial period in each layer [see Fig. 6(a1)]. The vortices move away from each other, their intensity decreases, and four additional vortices appear [Fig. 6(b1)]. The intensity of the ''new'' vortices grows, while that of the ''old'' vortices continues to decrease [Fig. 6(c1)]. Finally, the latter vortices disappear [Fig. 6(d1)]. After one-half of the time period, the structure is identical to the previous one, but it is shifted by one-half a spatial period:

$$\psi(x,z,t+\tau/2)=\psi(x+L/2,z,t),$$

$$T(x,z,t+\tau/2)=T(x+L/2,z,t),$$

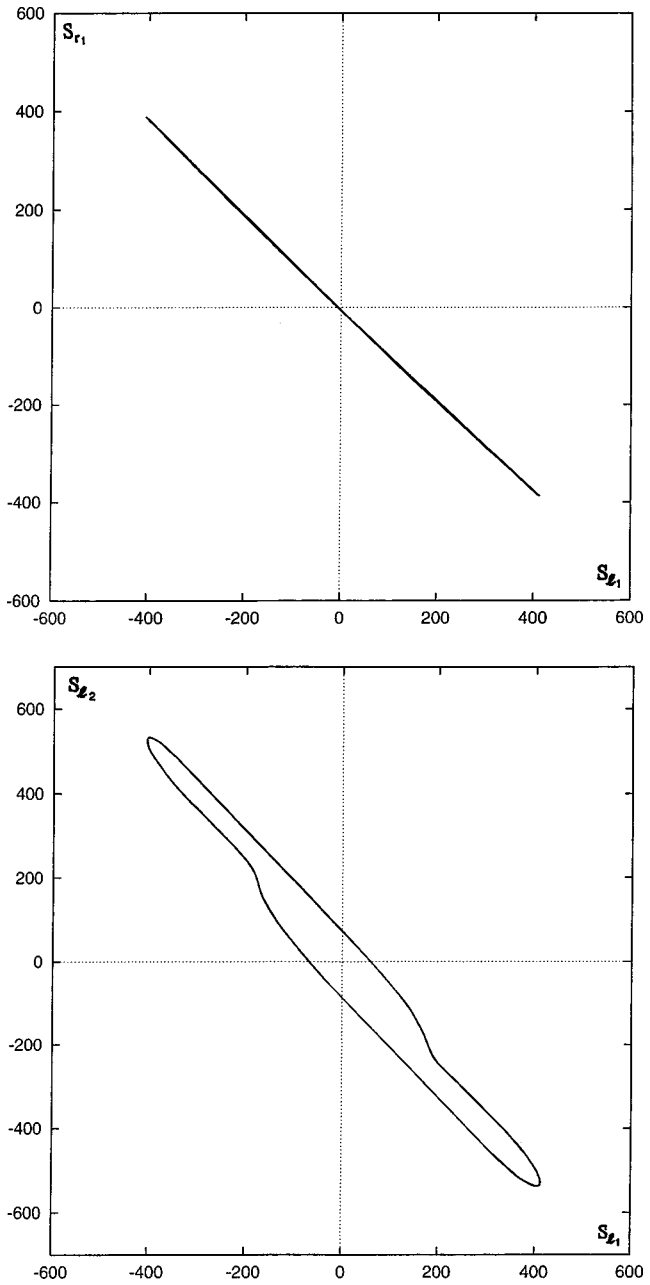

FIG. 7. Phase diagrams of the oscillatory motion; $M=3.07\times10^4$.

where τ is the time period.

In order to describe the spatial structure of the flow, we introduce the following integral variables characterizing the intensity of the motion in the left and in the right halves of the layers:

$$S_{l1}(t)=\int_0^{L/2}dx\int_0^1 dz\,\psi_1(x,z,t),$$

$$S_{r1}(t)=\int_{L/2}^{L}dx\int_0^1 dz\,\psi_1(x,z,t),$$

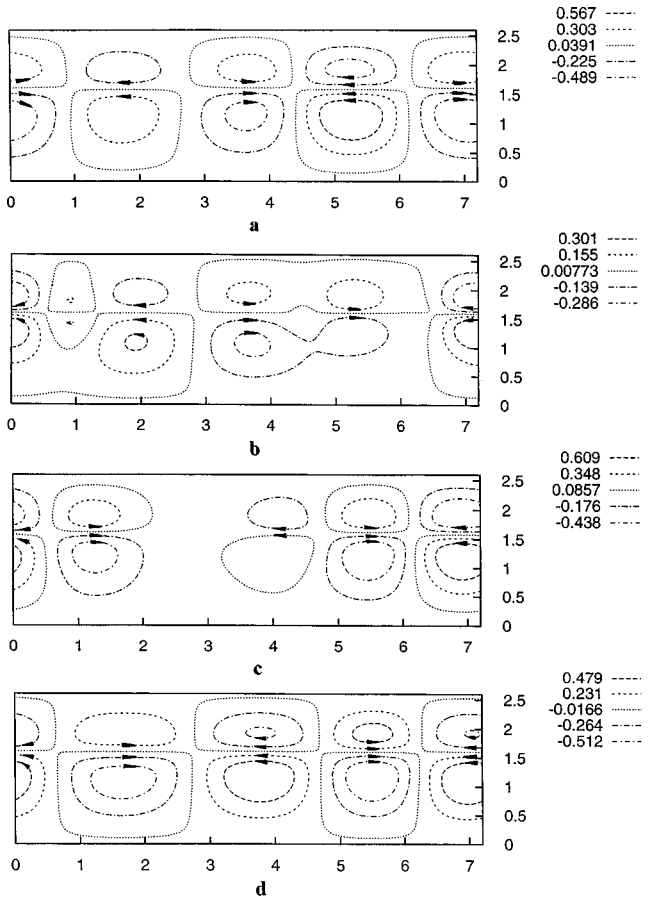

FIG. 8. Streamlines (a)–(d) for the asymmetric nonperiodic motion in the region with $L=7.2$; $M=3.07\times10^4$.

$$S_{l2}(t)=\int_0^{L/2}dx\int_0^1 dz\,\psi_2(x,z,t). \tag{32}$$

The phase trajectories in the variables (S_{l1},S_{r1}) and (S_{l1},S_{l2}) confirm the symmetry (31) of the oscillations [see Fig. 7(a)] and their periodicity [see Fig. 7(b)].

In accordance with the prediction of the weakly nonlinear theory, the oscillations were also observed in the subcritical region, where sufficiently small disturbances decay on the background of the mechanical equilibrium state, while some finite-amplitude disturbances generate a nondecaying oscillatory regime.

We also performed the calculations in a longer computational region $L=7.2$. It turns out that the regular standing wave is unstable with respect to the spatiotemporal modulation. We observed the same processes of creation and suppression of vortices as in the case $L=3.6$, but now they take place in an asymmetric, irregular way (see Fig. 8).

Rigid heat-insulated lateral boundaries

The nonlinear simulations of the finite-amplitude convective regimes were also performed in a system with rigid heat-insulated lateral boundaries [see the boundary conditions (30)]; $L=3.6$.

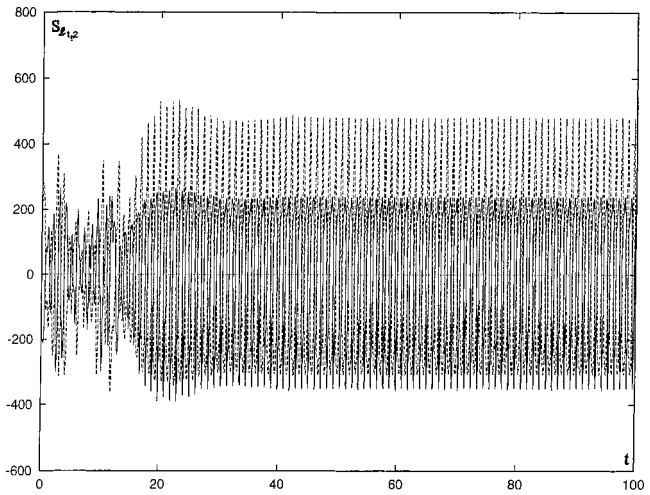

FIG. 9. The dependence of $S_{l1,2}(t)$ in the region with $L=7.2$; $M=5.03\times10^4$; Gr$=150$.

The oscillations turn out to be nonperiodic in time in the whole region where they have been observed, $M>2.65\times10^4$.

B. Influence of buoyancy on thermocapillary convection

Now let us consider the influence of buoyancy on nonlinear thermocapillary oscillations. The simulations were performed with periodic lateral boundaries [see Eq. (29)]. The inclusion of the Grashof number leads to regularization of the nonperiodic oscillations. The transition from the chaotic motion to regular oscillations is shown in Fig. 9. The phase trajectory after the transient period looks like a closed line (see Fig. 10). With increase of the Grashof number the oscillations are completely suppressed.

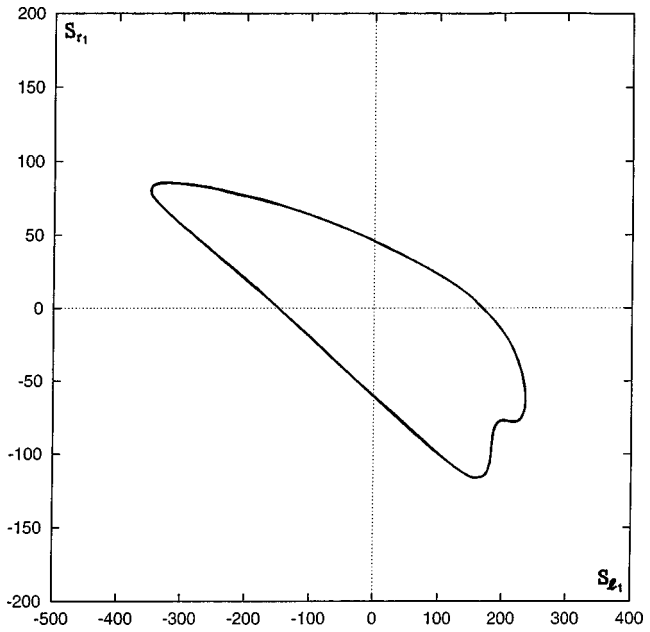

FIG. 10. The dependence of $S_{r1}(S_{l1})$ in the region with $L=7.2$; $M=5.03\times10^4$; Gr$=150$.

V. CONCLUSION

Linear and nonlinear simulations of oscillatory flow regimes have been performed for the real two-layer system *n*-octane–methanol. It is found that for a definite ratio of layer thicknesses the critical Marangoni number for the oscillatory instability has a minimum.

The prediction of the weakly nonlinear theory [8] is justified: standing waves have been observed in the subcritical region. It was found that at Gr$=0$ oscillations are never time periodic in a sufficiently long computational region.

The inclusion of buoyancy leads to regularization and finally to the complete suppression of oscillations. The oscillatory instability can be observed only under microgravity conditions.

[1] P. Colinet, J. C. Legros, and M. G. Velarde, *Nonlinear Dynamics of Surface-Tension-Driven Instabilities* (Wiley-VCH, Berlin, 2001).
[2] I. B. Simanovskii and A. A. Nepomnyashchy, *Convective Instabilities in Systems with Interface* (Gordon and Breach, London, 1993).
[3] C. V. Sternling and L. E. Scriven, AIChE J. **5**, 514 (1959).
[4] A. Rednikov, P. Colinet, M. Velarde, and J.-C. Legros, Phys. Rev. E **57**, 2872 (1998).
[5] J. Reichenbach and H. Linde, J. Colloid Interface Sci. **84**, 433 (1981).
[6] A. Nepomnyashchy and I. Simanovskii, Fluid Dyn. **18**, 629 (1983).
[7] A. Nepomnyashchy and I. Simanovskii, Sov. Phys. Dokl. **28**, 838 (1983).
[8] P. Colinet, Ph. Georis, J.-C. Legros, and G. Lebon, Phys. Rev. E **54**, 514 (1996).
[9] Ph. Georis and J. C. Legros (private communication).
[10] M. G. Velarde, A. A. Nepomnyashchy, and M. Hennenberg, Adv. Appl. Mech. **37**, 167 (2001).
[11] T. V. Kuskova and L. A. Chudov, Comput. Methods Programming **11**, 27 (1968) (in Russian).